Langmuir
Article
pubs.acs.org/Langmuir

Bioinspired Silica Surfaces with Near-Infrared Improved Transmittance and Superhydrophobicity by Colloidal Lithography

Yunfeng Li,[†] Junhu Zhang,[†] Shoujun Zhu,[†] Heping Dong,[‡] Fei Jia,[†] Zhanhua Wang,[†] Yue Tang,[†] Liang Zhang,[†] Shiyu Zhang,[†] and Bai Yang*[,†]

[†]*State Key Laboratory of Supramolecular Structure and Materials, College of Chemistry and* [‡]*College of Mathematics, Jilin University, Changchun 130012, P. R. China*

Received January 14, 2010. Revised Manuscript Received February 22, 2010

In this paper, we report a kind of bioinspired high performance near-infrared improved transmittance silica surfaces with superhydrophobic properties by colloidal lithography, with transmittance about 99% from 1300 to 2000 nm. Meanwhile, the optical properties of such surfaces can be controlled by the antireflective structure morphologies resulting from the different reactive ion etching conditions. Using proper microspheres as mask, the high-performance near-infrared telecommunication optics can be achieved. Besides, the antireflective surfaces possess superhydrophobic properties after modified by fluorosilane. Such antireflective surfaces are promising for fabrication of highly light transmissive, antireflective, and superhydrophobic near-infrared optical materials to be used in many important fields.

1. Introduction

Near-infrared (NIR) optical windows are indispensable in varieties of important practical applications, such as NIR telecommunication,[1] NIR high-power lasers,[2,3] night vision systems,[4] and sensors.[2] Unfortunately, optical elements based on fused silica with refractive index from 1.43 to 1.47 reflect about 4% of normal incident light from each air−substrate interface. The additive loss of reflection is especially detrimental to a system's performance. For example, in high-power laser systems, light reflected from windows, lasing crystals, and optics can cause the failure of laser components such as pump diodes, limiting the lifetime and the amount of laser energy that can be extracted. This in turn limits the range of laser communications systems and laser environmental sensors, and reduces the amount of laser energy delivered in medical lasers, laser weapons, and laser fusion systems. In addition, imaging systems such as cameras and NIR focal plane arrays have a vulnerability to reflected light from internal windows, imaging optics, and in particular the highly reflective surface of the detector arrays. These stray light reflections cause ghost images and increased background noise that both serve to reduce the sensor's effectiveness. Therefore, simultaneously suppressing reflection and increasing transmittance of light are very crucial to the performance of optical systems, especially when there are several optical elements involved. Despite the technical importance, actual material solutions for significant improvement are limited, especially in the infrared spectral region.[5] In practical applications, single or multilayered antireflective coatings[6−11] are widely used in many fields. However, such antireflective coatings demand that the optical thickness of the layers should increase with the designed wavelength increasing.[12] Thus, the antireflective coatings for NIR region would require thicker and more layers than those for the visible region. The preparation of such coating is in trouble due to difficulty of controlling the coating conditions and homogeneity of the coatings. In the field of infrared optics, refractive indices of optical materials are very high and the proper materials for antireflective coatings based on multilayered films are rare in nature. Besides, the antireflective coatings suffer from the problems of cracking or peeling from the substrates due to the thermal strain caused by NIR optical radiation.[1]

Nature gives us some inspiration to solve the problems mentioned above. An astonishing variety of natural photonic structures exist,[13−17] such as the iridescent color of butterfly wings, beetles, and peacock tail, photocollector in brittlestar, and antireflection in insect compound eyes and wings. Some nocturnal insects use nipple arrays of sub-300-nm size as antireflective structures (ARS) to reduce reflection from their compound eyes. The ARS on the corneas of these insects can improve sensitivity of light vision by increasing transmittance of light in dark condition. Stavenga and co-workers have investigated in detail the structures and optical properties of the moth-eye corneal nipple arrays of the facet lenses of 19 diurnal butterfly species.[13] The corneal nipples locally are arranged in a highly regular, hexagonal lattice. They found that the nipple arrays of different species exhibit different morphologies, such as height, profile, and base diameter. Besides,

*To whom the correspondence should be addressed. Fax: +86 431 85193423. E-mail: byangchem@jlu.edu.cn.

(1) Kulakofsky, J.; Lewis, W.; Robertson, M.; Moore, T.; Krishnan, G. *Proc. SPIE* **2001**, *4679*, 198–210.
(2) Hobbs, D. S.; MacLeod, B. D.; Riccobono, J. R. *Proc. SPIE* **2007**, *6545* (65450Y), 1–14.
(3) Xu, Y.; Zhang, L.; Wu, D.; Sun, Y. H.; Huang, Z. X.; Jiang, X. D.; Wei, X. F.; Li, Z. H.; Dong, B. Z.; Wu, Z. H. *J. Opt. Soc. Am. B* **2005**, *22*, 905–912.
(4) Zhang, L. B.; Li, Y.; Sun, J. Q.; Shen, J. C. *J. Colloid Interface Sci.* **2008**, *319*, 302–308.
(5) Kikuta, H.; Toyota, H.; Yu, W. *Opt. Rev.* **2003**, *10*, 63–73.
(6) Hiller, J. A.; Mendelsohn, J. D.; Rubner, M. F. *Nat. Mater.* **2002**, *1*, 59–63.
(7) Xi, J. -Q.; Schubert, M. F.; Kim, J. K.; Schubert, E. F.; Chen, M. F.; Lin, S. Y.; Liu, W.; Smart, J. A. *Nature Photon* **2007**, *1*, 176–179.
(8) Walheim, S.; Schäffer, E.; Mlynek, J.; Steiner, U. *Science* **1999**, *283*, 520–522.
(9) Dobrowolski, J. A.; Guo, Y. E.; Tiwald, T.; Ma, P. H.; Poitras, D. *Appl. Opt.* **2006**, *45*, 1555–1562.
(10) Koo, H. Y.; Yi, D. K.; Yoo, S. J.; Kim, D. Y. *Adv. Mater.* **2004**, *16*, 274–277.
(11) Lee, D.; Rubner, M. F.; Cohen, R. E. *Nano Lett.* **2006**, *6*, 2305–2312.
(12) Biswas, P. K.; Kundu, D.; Ganguli, D. *J. Mater. Sci. Lett.* **1989**, *8*, 1436–1437.
(13) Stavenga, D. G.; Foletti, S.; Palasantzas, G.; Arikawa, K. *Proc. R. Soc. B* **2006**, *273*, 661–667.
(14) Srinivasarao, M. *Chem. Rev.* **1999**, *99*, 1935–1961.
(15) Miller, W. H.; Bernard, G. D.; Allen, J. L. *Science* **1968**, *162*, 760–767.
(16) Parker, A. R.; Townley, H. E. *Nat. Nanotechnol.* **2007**, *2*, 347–353.
(17) Vukusic, P.; Sambles, J. R. *Nature* **2003**, *424*, 852–855.

they used different optical models to calculate the performance of antireflective properties of them. The nipple arrays create an interface with a gradient refractive index between that of air and the facet lens material, and can suppress the reflection of light from the corneal surface. On the basis of such principles, fabrication of subwavelength ARS (moth's eye structures) directly on the surface of silicon[18−20] and other semiconductors[21,22] has been reported. Similar to the nipple arrays in insects' compound eyes and wings,[13] the ARS surfaces with nipple-like or tapered profiles exhibit a gradient in refractive index between air and substrate. Therefore, they can dramatically suppress the reflection losses at the interface over a large range of wavelength and a large field of view.[23,24] The ARS surfaces exhibit distinct advantages compared to coatings. The ARS surfaces exhibit higher mechanical stability and better durability than coatings because no foreign materials are involved.[5] Moreover, the ARS surfaces are free of the problem of peeling from the substrates when they are used over a broad temperature range. As a result, the ARS surfaces are highly desired for NIR optical applications.

Many techniques based on top-down lithography, such as electron-beam etching,[25] fast atom beam,[26] and interference lithography,[27,28] have been applied to prepare ARS surfaces. However, conventional top-down lithographic technologies require sophisticated equipments and are time-consuming and expensive for large area fabrication in practical applications. For ultraviolet and visible light applications, in order to eliminate scattering of light, feature sizes of bioinspired nipple arrays below 200 nm are always necessary, which are on the scale of nipple arrays on the corneas of moths. For NIR light applications, feature sizes of ARS are in the 500 nm to 1.5 μm range. Recently, by inspiring the nipple arrays on the corneas of moths, NIR ARS surfaces on silicon[29] prepared by nanosphere lithography have been reported, but there are few ARS surfaces on the fused silica for NIR improved transmission of light applications.

For NIR optical applications in night vision systems and NIR spectrum analysis work,[30] the harmful influence of water vapor existing in the external environment is significant for the performance of antireflective coatings. Therefore, fabrication of ARS surfaces with superhydrophobic properties is highly desired in many practical applications. The ordered microstructure arrays on the compound eyes of insects exhibit both antireflective and superhydrophobic properties.[31] Recently, multifunctional antireflective surfaces[29] have attracted a lot of interest due to improvement of optical device performance. For instance, we have successfully prepared high aspect ratio silicon hollow-tip arrays for antireflective and water-repellent surfaces.[32] Such antireflective surfaces with water-repellent properties enable the applications of them in humid environment.

In our past work, we reported a simple and time-efficient method to prepare large area fused silica cone arrays on planar fused silica substrate and planconvex lens for high-performance visible light ARS and antifogging surfaces.[33] The ARS surfaces dramatically suppressed the surface-reflective loss in visible light region with incidence angle up to 45°. Besides, such surfaces exhibited high performance antifogging properties. In this paper, high performance NIR antireflective and improved transmittance surfaces are reported. The optical properties of the ARS surfaces can be controlled by the ARS morphologies resulting from the different reactive ion etching conditions. High performance NIR telecommunication optics can be achieved using proper microspheres as mask. Besides, the ARS surfaces possess superhydrophobic properties after modified by fluorosilane. Due to the time-efficient and reproducible preparing process, the ARS surfaces are promising for many important applications, such as NIR high-power lasers, optical lenses, NIR spectrum, NIR shielding field, and night vision system.

2. Experimental Section

Materials. Polystyrene (PS) microspheres were prepared by emulsion polymerization as mentioned in reference.[34] The PS microspheres used in our work were 580 nm, 436 nm, and 210 nm in diameter, respectively. The fused silica substrates were cut into 20 mm × 10 mm pieces, soaked in the mixture of 98% H_2SO_4/30% H_2O_2 (volumetric ratio 7:3) for 20 min under boiling (caution: strong oxide), and then rinsed with deionized water several times and dried with N_2 stream. All the chemical reagents in our work were used as received.

Fabrication. The monolayer PS microspheres were prepared by interface method. In brief, 0.1 mL of 0.5% PS microsphere dispersion in a mixture of deionized water and absolute ethanol (v/v, 1:1) was dropped on the surface of the water in the 12 cm diameter glass tank, and then 20 μL of 5% sodium lauryl sulfate solution was added; finally, the monolayer microspheres were lifted up onto the silica substrate, and the 2D colloidal crystals were obtained when the slides were dry. The silica ARS were fabricated by RIE. The RIE process were performed using a 2:3 mixture of Ar and CF_4 as a process gas at a total flow rate of 50 sccm, chamber pressure 40 mTorr, and RF power 300 W. Etching time was from 4 to 40 min. For fabricating two side silica ARS arrays, the silica substrate with one side silica ARS array was used as substrate to fabricate PS colloidal crystals, and then the two side silica ARS arrays were fabricated by RIE.

Characterization. SEM micrographs were taken with a JEOL FESEM 6700F electron microscope with primary electron energy of 3 kV. The samples were sputtered with a thin layer of Pt prior to imaging. A Shimadu 3600 UV−vis-NIR spectrophotometer with standard mirror optics was used to measure the specular reflectance in the 400−2500 nm range at the incidence angle of 5°. The transmittance was measured using Shimadu 3600 UV−vis-NIR spectrophotometer at normal incidence. Before measuring the water contact angles (CA), the silica ARS arrays were performed in the oxygen plasma to make the surface of arrays hydrophilic, and then put in the sealed jar with a little amount of trichloro-(1*H*,1*H*,2*H*,2*H*-perfluorooctyl) silane (Aldrich) at 60 °C for 6 h.

(18) Lee, C.; Bae, S. Y.; Mobasser, S.; Manohara, H. *Nano Lett*. **2005**, *5*, 2438–2442.
(19) Chen, H. L.; Chuang, S. Y.; Lin, C. H.; Lin, Y. H. *Opt. Express* **2007**, *15*, 14793–14803.
(20) Zhu, J.; Yu, Z. F.; Burkhard, G. F.; Hsu, C. M.; Connor, S. T.; Xu, Y. Q.; Wang, Q.; McGehee, M.; Fan, S. H.; Cui, Y. *Nano Lett*. **2009**, *9*, 279–282.
(21) Chattopadhyay, S.; Chen, L. C.; Chen, K. H. *Crit. Rev. Solid State Mater. Sci*. **2006**, *31*, 15–53.
(22) Diedenhofen, S. L.; Vecchi, G.; Algra, R. E.; Hartsuiker, A.; Muskens, O. L.; Immink, G.; Bakkers, E. P. A. M.; Vos, W. L.; Rivas, J. G. *Adv. Mater*. **2009**, *16*, 973–978.
(23) Huang, Y. F.; Chattopadhyay, S.; Jen, Y. J.; Peng, C. Y.; Liu, T. A.; Hsu, Y. K.; Pan, C. L.; LO, H. C.; Hsu, C. H.; Chang, Y. H.; Lee, C. S.; Chen, K. H.; Chen, L. C. *Nat. Nanotechnol*. **2007**, *2*, 770–774.
(24) Lohmüller, T.; Helgert, M.; Sundermann, M.; Brunner, R.; Spatz, J. P. *Nano Lett*. **2008**, *8*, 1429–1433.
(25) Toyota, H.; Takahara, K.; Okano, M.; Yotsuya, T.; Kikuta, H. *Jpn. J. Appl. Phys*. **2001**, *40*, L747–L749.
(26) Kanamori, Y.; Kikuta, H.; Hane, K. *Jpn. J. Appl. Phys*. **2000**, *39*, L735–L737.
(27) Clapham, P. B.; Hutley, M. C. *Nature* **1973**, *244*, 281–282.
(28) Wilson, S. J.; Hutley, M. C. *Opt. Acta* **1982**, *29*, 993–1009.
(29) Min, W. L.; Jiang, B.; Jiang, P. *Adv. Mater*. **2008**, *20*, 3914–3918.
(30) McClure, W. F. *J. Near Infrared Spec*. **2003**, *11*, 487–518.
(31) Watson, G. S.; Watson, J. A. *Appl. Surf. Sci*. **2004**, *235*, 139–144.
(32) Li, Y. F.; Zhang, J. H.; Zhu, S. J.; Dong, H. P.; Wang, Z. H.; Sun, Z. Q.; Guo, J. R.; Yang, B. *J. Mater. Chem*. **2009**, *19*, 1806–1810.
(33) Li, Y. F.; Zhang, J. H.; Zhu, S. J.; Dong, H. P.; Jia, F.; Wang, Z. H.; Sun, Z. Q.; Zhang, L.; Li, Y.; Li, H. B.; Xu, W. Q.; Yang, B. *Adv. Mater*. **2009**, *21*, 4731–4734.
(34) Zhang, J. H.; Chen, Z.; Wang, Z. L.; Zhang, W. Y.; Ming, N. B. *Mater. Lett*. **2003**, *57*, 4466–4470.

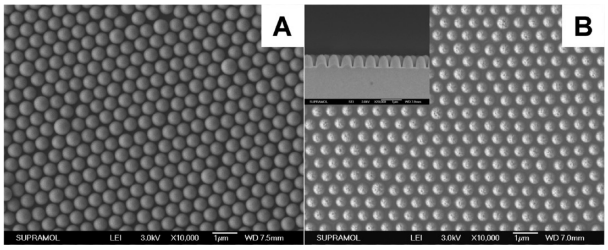

Figure 1. (A) SEM images of 2D colloidal crystals used as masks. (B) The morphology of silica ARS arrays by RIE etching 20 min; the inset is the cross-sectional SEM images of them. All the scale bars are 1 μm.

The water CA is measured using a KRUSS DSA 100 contact angle goniometer. Each reported contact angle is the average of five measurements. The static contact angles were read by injecting 4 μL water.

3. Results and Discussion

3.1. Fabrication of Bioinspired Silica ARS Arrays. The ARS surfaces were prepared by colloidal lithography.[35] First, 2D colloidal crystals of polystyrene (PS) microspheres were prepared by modified interface method.[36] Subsequently, silica ARS arrays were prepared by a short-term reactive ion etching (RIE) using 2D PS colloidal crystals as masks. To fabricate double-sided ARS surfaces, the silica substrate with single-sided ARS surfaces was used as substrate to fabricate 2D PS colloidal crystals, and then the double-sided ARS surfaces were fabricated by RIE.

Figure 1A shows the 2D PS colloidal crystals that we used as masks, with PS microspheres 580 nm in diameter. We can see that the packing order of PS microspheres is face-centered cubic (fcc) lattice with the (111) plane parallel to the surface of the substrate. The ARS surfaces were prepared by RIE process. As shown in Figure 1B, nipple-like protuberance arrays were etched into the substrate. Remarkably, the nipple arrays are hexagonally non-close-packed just like the nipple arrays on the cornea of moth, and the root diameter of the nipple is about 504 nm. The cross-sectional images (the inset of Figure 1B) display the tapered profile. The nipple arrays are vertical to the substrate with 580 nm in period and 604 nm in height.

Using colloidal lithography, the morphologies of ARS can be easily controlled with different etching time. By changing the experimental conditions, we have arbitrarily prepared ARS with different morphologies: from postlike profile, truncated cone-shaped profile, paraboloid-like profile to pillar arrays with cone top profile. Figure 2 shows the morphology evolution of ARS with 580 nm in period as etching time increasing. After 4 min RIE etching, silica postlike arrays (Figure 2A,B) were etched into the substrate, with 194 nm in height, and the tops of them were smooth. Figure 2C,D shows the SEM images of ARS after 11 min etching. From them, we can see that the ARS exhibit truncated cone-shaped profile vertical to substrate with 563 nm in height, and the tops of them were rough. After 23 min etching, the ARS show a paraboloid-like profile (Figure 2E,F) with 616 nm in height, and the tops became smoother than those of 11 min. For 40 min etching, the ARS change into pillar arrays with cone top (Figure 2G,H) 547 nm in height.

In order to trace the morphological evolution of the ARS, we prepared the ARS with different etching time. Figure 3 show the time dependency of height and distance between ARS with

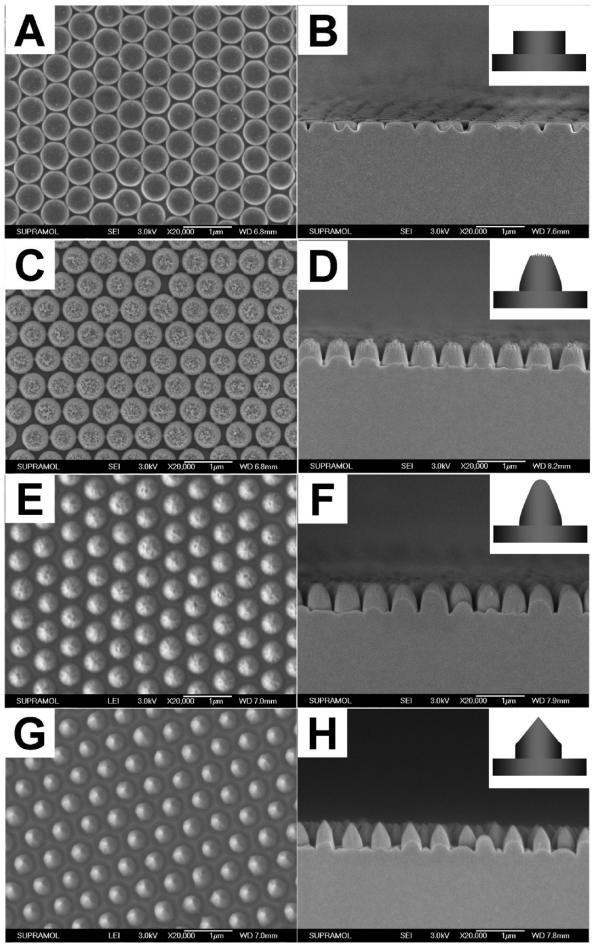

Figure 2. Morphology of silica ARS arrays by etching 4 min (A, B), 11 min (C, D), 23 min (E, F), and 40 min (G, H). All the scale bars are 1 μm. The insets are the schematic illustrations of different ARS.

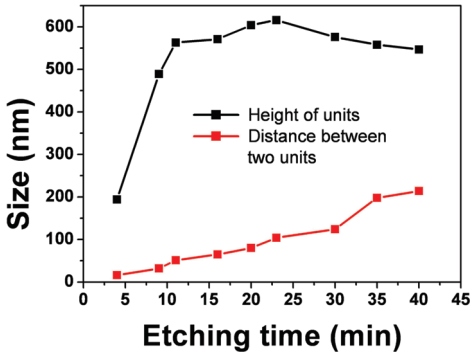

Figure 3. Time dependency of height and distance between two silica ARS with 580 nm in period.

580 nm in period. As the etching time increases, the height of ARS increases, and then decreases after about 23 min etching; however, the distance between ARS increases all the time. Through careful study of the morphologies of the ARS with different RIE time, the formation mechanism of the ARS arrays can be explained as follows. In the process of RIE, the PS microspheres are masks, but they can also be etched by the reactive ions. In the beginning, after 4 min RIE the silica postlike arrays (Figure 2A,B) are formed after removing the left spheres. During the etching, the diameter of the PS microspheres reduces

(35) Deckman, H. W.; Dunsmuir, J. H. *Appl. Phys. Lett.* **1982**, *41*, 377–379.
(36) Rybczynski, J.; Ebels, U.; Giesig, M. *Colloids Surf., A* **2003**, *219*, 1–6.

and the tops of spheres become rough[37] owing to the etching of ions during RIE process (Supporting Information, Figure S1), which leads to formation of truncated cone-shaped profile arrays with relatively smooth tops at 10 min etching after removing the left spheres (Supporting Information, Figure S2). In our work, we found that the spheres were completely removed after 11 min etching (Supporting Information, Figure S3). After the PS microspheres are removed by reactive ions completely, the silica truncated cone-shaped profile arrays with rough tops (Figure 2C,D) are obtained owing to the rough top masks. As the etching time continues, the tops of ARS will become smooth due to the direct etching of ions. Moreover, the tops, which are nearer to the plasma, are etched more rapidly than the narrow bottom areas between the posts.[38] As a result, the paraboloid-like arrays were obtained (Figure 2E,F). Continuously increasing the etching time, the over etching will happen to the ARS arrays, which leads to formation of pillar arrays with cone top (Figure 2G,H).

Through colloidal lithography, we can easily prepare the ARS arrays with different periods using different 2D colloidal crystals as masks. Supporting Information Figure S4 shows the tilted SEM images of ARS arrays with 210 nm (Supporting Information Figure S4A) and 436 nm (Supporting Information Figure S4B) in period. We can see that the morphology of them is almost the same, just like the nipple arrays on the corneas of moth eyes.

3.2. Antireflective Properties of Bioinspired Silica ARS Arrays. The ARS surfaces have similar morphologies with the nipple arrays on cornea of moth, which dramatically suppress the reflection loss and increase the transmittance of light.[13] The optical performance of the ARS surfaces presented here was evaluated by transmittance and reflection measurements in the 400−2500 nm range. The specular reflection was measured at an incidence angle of 5°, while the transmittance was measured at normal incidence. Figure 4 shows the antireflective properties of the ARS surfaces. From it, we can see that the different morphologies of ARS surfaces exhibit different antireflective properties. The specular reflection of double-sided ARS surfaces with paraboloid-like profile exhibits reflectance below 2.5% over the spectral range 800−2500 nm (the magenta line in Figure 4A), while the specular reflection of planar silica substrate is above 8% (the black line in Figure 4A). The specular reflection of postlike arrays and pillar arrays with cone top are both above the specular reflection of paraboloid-like arrays, but below the specular reflection of planar silica substrate. The transmittance of double-sided ARS surfaces with paraboloid-like profile is >99% from 1600 to 2130 nm, with transmittance maximum 99.38% at 1868 nm (the magenta line in Figure 4B), while the transmittance of planar silica substrate is <93% (the black line in Figure 4B). At the same time, the transmittance of postlike arrays and pillar arrays with cone top are both above the transmittance of planar silica substrate and below the transmittance of paraboloid-like arrays. Comparing Figure 4A,B, we can see that the improved transmittance is in accordance with the reduced reflectance. So, it is apparent that light scattering and absorption loss, introduced by fabricating process, play a minor role.

In order to interpret the antireflective properties of different ARS morphologies, the refractive index profiles of them were determined by theoretical simulation[39] (Figure 5). For surface antireflective properties, the gradual change of the refractive index from air to bulk is crucial. According to the theory

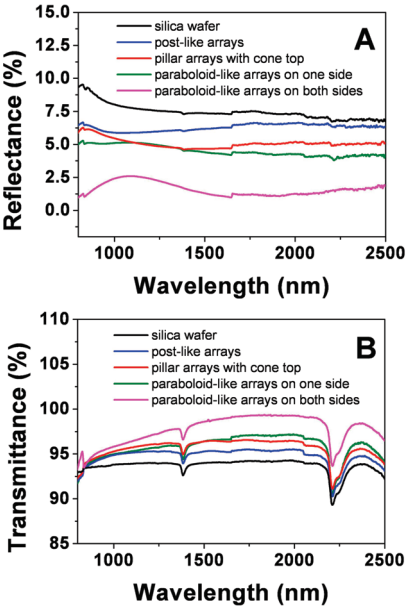

Figure 4. High performance antireflective properties of the silica ARS arrays. (A) Reflection of different silica ARS arrays. (B) Transmittance of different silica ARS arrays.

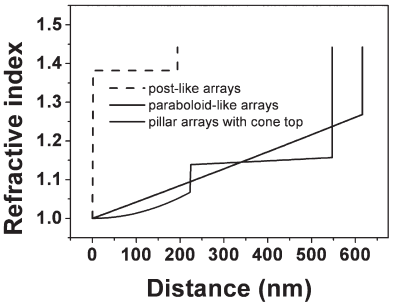

Figure 5. Gradient refractive index profile simulation of ARS surfaces from the peaks to the troughs (λ = 1681 nm).

analysis,[28] the transition of the refractive index is steadier, the surface reflection is less. For planar silica substrate, the refractive index is sharply changed from 1.0 to 1.442 (at 1681 nm) across the air/silica interface, resulting in high reflection (Figure 4A). For the silica substrate with postlike arrays, the effective index also sharply changed from 1.0 to 1.382, and then sharply to 1.442, leading to high reflection too, but the reflection of them is smaller than that of planar silica substrate (Figure 4A). For ARS surfaces of pillar arrays with cone top,[40] the effective index is continuously changed from 1.0 to 1.068, then sharply to 1.139, and at last sharply to 1.442. Although the reflection of them is smaller than that of the ARS surfaces with postlike arrays, the antireflective properties are suboptimal due to the abrupt transition of refractive index. The solid black line in Figure 5 shows the effective refractive index profile of the ARS surfaces with paraboloid-like arrays. The effective index of them is continuously changed from 1.0 to 1.269, and then sharply to 1.442. As a result, such surfaces show the best antireflective properties. However, there is also a little reflective loss on the ARS surfaces with paraboloid-like arrays due to the sharp transition of refractive index at the interface of array roots and silica bulk. The antireflective property of as-prepared ARS surfaces is better than that of nipple arrays on

(37) Fujimura, T.; Tamura, T.; Itoh, T.; Haginoya, C.; Komori, Y.; Koda, T. *Appl. Phys. Lett.* **2001**, *78*, 1478–1480.
(38) Okuyama, S.; Matsushita, S. I.; Fujishima, A. *Langmuir* **2002**, *18*, 8282.
(39) Macleod, H. A. *Thin-Film Optical Filters*; Institute of Physics Publishing: Bristol, 2001; pp 40−42.
(40) Wu, H. M.; Lai, C. M.; Peng, L. H. *Appl. Phys. Lett.* **2008**, *93*(211903), 1–3.

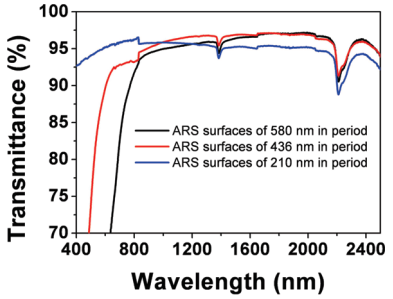

Figure 6. Transmittance for ARS surfaces of different period.

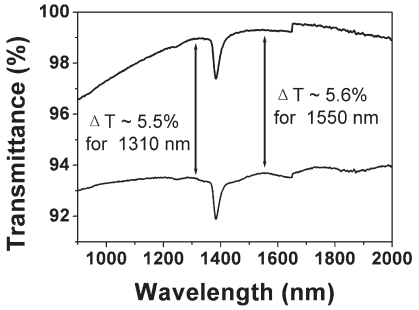

Figure 7. High performance antireflective surfaces for NIR telecommunication optics. The black line is the transmittance of double-sided ARS surfaces, and the gray line is the transmittance of silica substrate.

the corneal of moth, because the refractive index profile of as-prepared ARS is steadier than that of nipple arrays on the corneal of moth.

The antireflective properties of ARS surfaces are not only broadband, but in addition, the best antireflective wave bands depend on the period of ARS arrays.[41] Figure 6 shows the transmittance of paraboloid-like ARS arrays with different period. We can see that the best wave bands of ARS surfaces red-shift with the periods of ARS arrays increasing. For ARS surfaces with 210 nm in period, the best wave band is in the visible light region, while for ARS surfaces with 436 and 580 nm in period, the best wave bands are in the near-infrared region. Utilizing such mechanism, we prepared high-performance antireflective surfaces for NIR optical communication applications. For the double-sided ARS surfaces with paraboloid-like arrays of 436 nm in period, the transmittance at 1310 nm is 98.9%, and at 1550 nm is 99.3% (Figure 7); while improvement of transmittance is 5.5% at 1310 nm, and about 5.6% at 1550 nm. Compared to thin film antireflective coatings, ARS surfaces exhibit high-quality mechanical stability and durability, because they are free of mechanical adhesion problems and tensile stress when they are used over a broad thermal range. Especially for high power components in optical telecommunications, the temperature of element surfaces will increase; however, the ARS surfaces are free of cracking or peeling from substrate caused by the thermal mismatch, because no foreign materials involved.

3.3. Superhydrophobic Properties of Bioinspired Silica ARS Arrays. The ARS arrays on eyes of insects exhibit both antireflective and superhydrophobic properties.[31] The silica ARS arrays could also significantly enhance the hydrophobicity of the surface after modified fluorosilane due to the high fraction of air

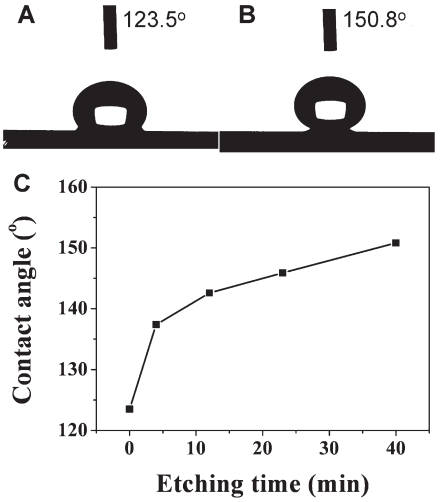

Figure 8. Static contact angle of silica wafer (A) and silica ARS arrays by RIE etching 40 min (B). (C) Contact angles with different etching time.

trapped in the trough area between arrays.[42] Figure 8B shows the water droplet profile on fluorosilane modified silica ARS surfaces with 580 nm in period, and the measured apparent water contact angle is ca. 150.8° for ARS surfaces 40 min RIE etching, significantly increased from ca. 123.5° on fluorinated flat silica wafer (Figure 8A). Besides, the water droplet can easily slide with no residual water when the substrate is tilted. From Figure 8C, we can see that the static contact angles increase with etching time increasing. We can use the Cassie−Baxter equation:[43] $\cos\theta_r = f_1 \cos\theta - f_2$ to interpret the evolution of contact angles, in which θ is the contact angle on planar silica substrate, θ_r is the contact angle on the ARS surfaces, f_1 and f_2 are the fractions of solid surface and air in contact with liquid, respectively (i.e., $f_1 + f_2 = 1$). As the etching time is increasing, the fraction of air trapped in the trough area between arrays increases. As a result, the contact angle of ARS surfaces increases with the etching time increasing.

4. Conclusions

In summary, we have prepared high performance NIR optical surfaces with superhydrophobic properties by colloidal lithography. Such surfaces dramatically suppress reflection over a large range of wavelength; at the same time, the transmittance substantially increases from 800 to 2500 nm. The optical properties of the ARS surfaces can be controlled by the ARS morphologies resulting from the different reactive ion etching conditions. More importantly, we can prepare high-performance optical windows for NIR optical telecommunication applications, the transmittance of 1310 and 1550 nm was dramatically enhanced by using proper 2D colloidal crystals as mask. Besides, the ARS surfaces possess superhydrophobic properties after modification by fluorosilane. Such NIR optical surfaces with superhydrophobic properties enable applications in humid environment. Compared to thin film antireflective coatings, the ARS surfaces exhibit high-quality mechanical stability and durability due to freedom from mechanical adhesion problems and tensile stress caused by thermal mismatch, especially in the NIR region. Because of the simple, time-efficient, and reproducible preparing process, such ARS surfaces are promising for fabrication of highly light transmissive, antireflective, and superhydrophobic NIR optical materials to be used for NIR high-power lasers, NIR

(41) Boden, S. A.; Bagnall, D. M. *Appl. Phys. Lett.* **2008**, *93*(133108), 1–3.
(42) Sun, T. L.; Feng, L.; Gao, X. F.; Jiang, L. *Acc. Chem. Res.* **2005**, *38*, 644–652.
(43) Cassie, A. B. D.; Baxter, S. *Trans. Faraday Soc.* **1944**, *40*, 546–561.

telecommunication, optical lenses, NIR spectrum, sensors, NIR shielding field, and night vision system applications.

Acknowledgment. This work was supported by the National Science Foundation of China (grant no. 20921003, 20534040, 20874039) and the National Basic Research Program of China (2007CB936402).

Supporting Information Available: The morphologies of spheres after RIE process; the morphologies of the bioinspired ARS arrays after reactive ion etching 10 min; the bioinspired silica ARS arrays after 11 min etching; SEM images of silica ARS arrays with different period. This material is available free of charge via the Internet at http://pubs.acs.org.